Supporting Information

Structure-activity correlation in aerobic cyclohexene oxidation and peroxide decomposition over $Co_xFe_{3-x}O_4$ spinel oxides

Julia Büker,[a] Steven Angel,[b] Soma Salamon,[c] Joachim Landers,[c] Tobias Falk,[a] Heiko Wende,[c] Hartmut Wiggers,*[b] Christof Schulz,[b] Martin Muhler,[a],[c] and Baoxiang Peng*[a],[c]

[a] Laboratory of Industrial Chemistry, Ruhr University Bochum, 44780 Bochum, Germany

[b] IVG, Institute for Combustion and Gas Dynamics – Reactive Fluids and CENIDE Center for Nanointegration, University of Duisburg-Essen, 47057 Duisburg, Germany

[c] Faculty of Physics, University of Duisburg-Essen, 47048 Duisburg, Germany

[d] Max Planck Institute for Chemical Energy Conversion, 45470 Mülheim an der Ruhr, Germany

E-mail: hartmut.wiggers@uni-due.de (H. Wiggers);

baoxiang.peng@techem.rub.de (B. Peng)

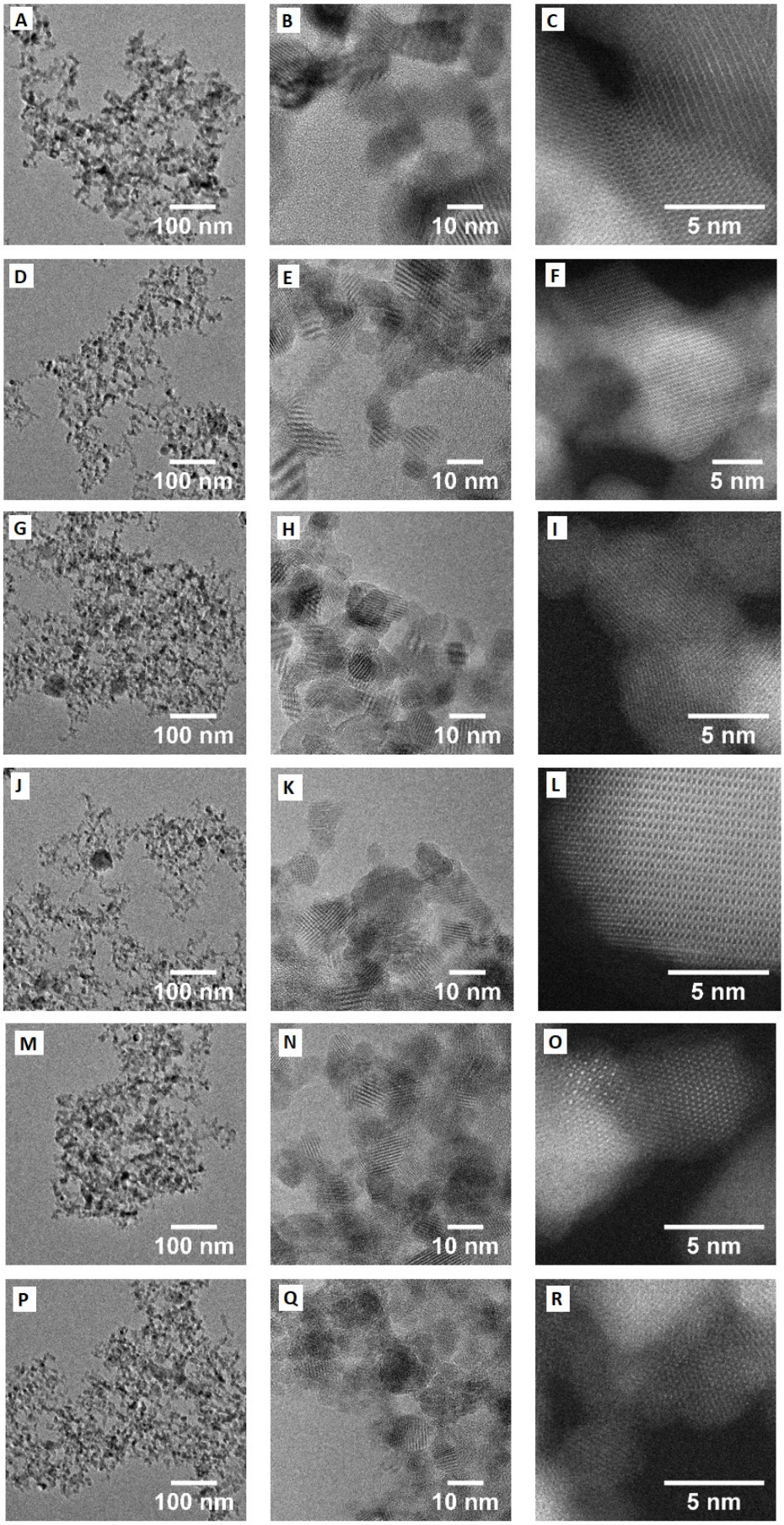

Figure S1. TEM and HAADF-STEM images of the $Co_xFe_{3-x}O_4$ (x=0, 0.5, 1, 1.5, 2, 2.5, 3) samples: Co_3O_4 (A-C), $Co_{2.5}Fe_{0.5}O_4$ (D-F), Co_2FeO_4 (G-I), $Co_{1.5}Fe_{1.5}O_4$ (J-L), $Co_{0.5}Fe_{2.5}O_4$ (M-O), γ-Fe_2O_3 (P-R).

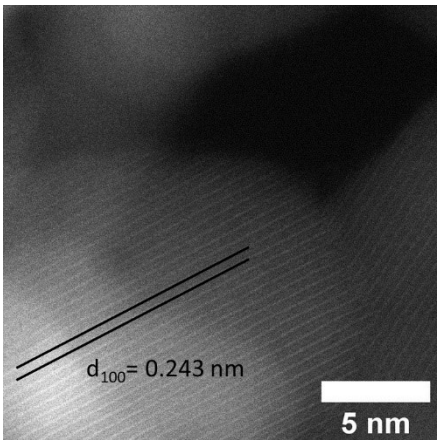

Figure S2. Determination of the lattice spacing in a Co_3O_4 particle.

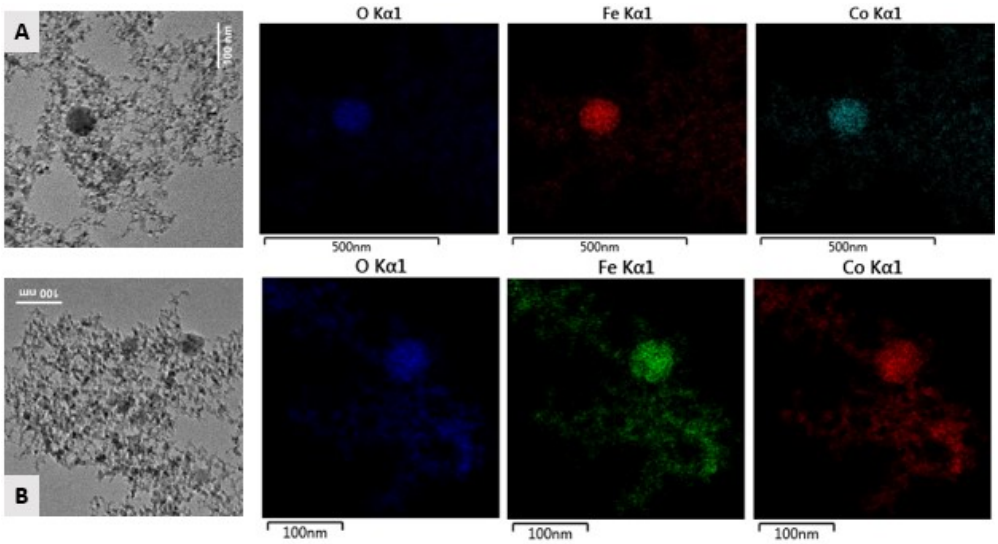

Figure S3. EDX mapping of Co_2FeO_4 (A) and $CoFe_2O_4$ (B).

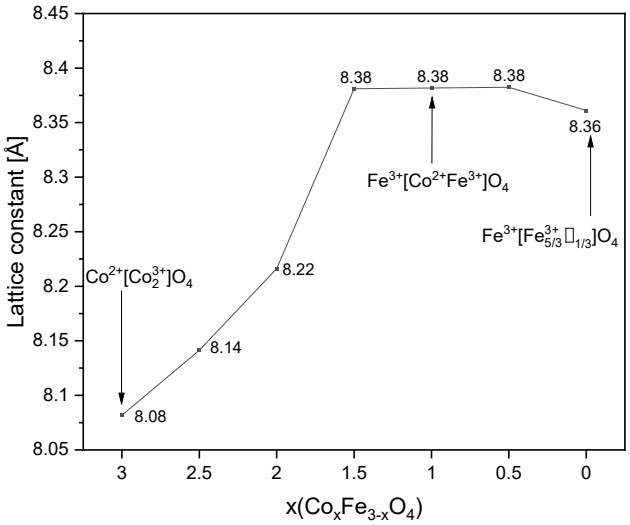

Figure S4. Lattice parameters of the $Co_xFe_{3-x}O_4$ (x=0, 0.5, 1, 1.5, 2, 2.5, 3) samples determined by Rietveld refinement.

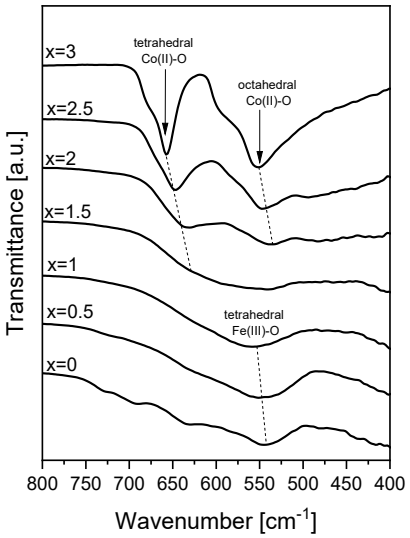

Figure S5. FT IR spectra of the $Co_xFe_{3-x}O_4$ (x=0, 0.5, 1, 1.5, 2, 2.5, 3) samples.

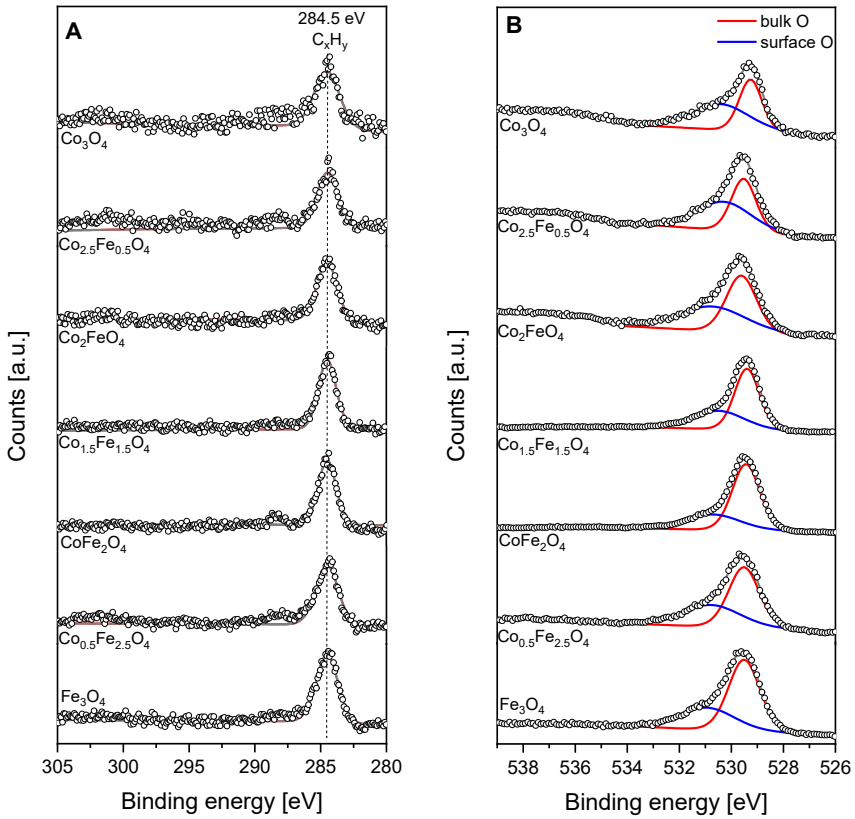

Figure S6. XP spectra of the C 1s (A) and O 1s (B) region of the $Co_xFe_{3-x}O_4$ (x=0, 0.5, 1, 1.5, 2, 2.5, 3) samples.

Table S1. Surface composition of the $Co_xFe_{3-x}O_4$ (x=0, 0.5, 1, 1.5, 2, 2.5, 3) samples derived from XP spectra.

Sample	C [at. %]	O [at. %]	Fe [at. %]	Co [at. %]
Co_3O_4	26.6	54.5	0	18.9
$Co_{2.5}Fe_{0.5}O_4$	22.6	56.6	3.4	17.4
Co_2FeO_4	27.6	54.9	5.6	11.9
$Co_{1.5}Fe_{1.5}O_4$	17.4	54.5	13.2	14.2
$CoFe_{2.5}O_4$	18.2	56.8	16.1	9.0
$Co_{0.5}Fe_{2.5}O_4$	30.3	54.7	12.2	2.8
γ-Fe_2O_3	33.1	52.5	14.5	0

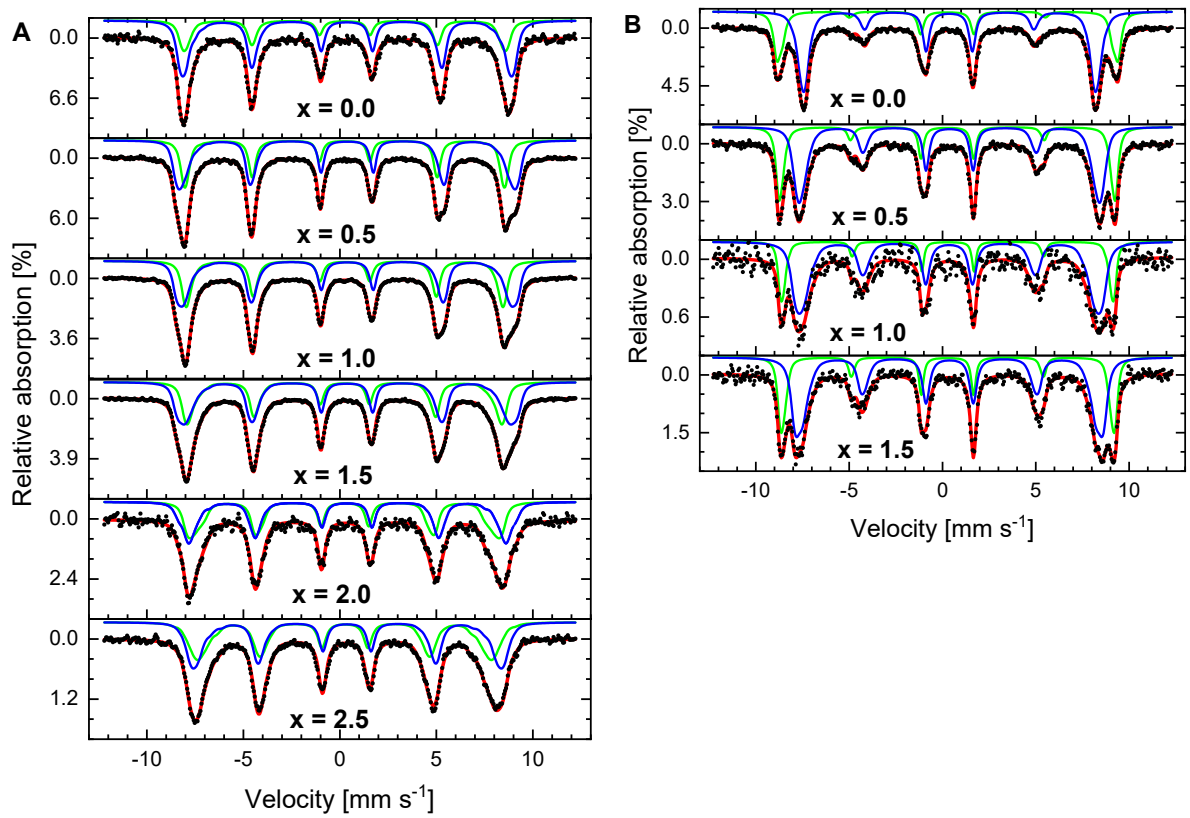

Figure S7. Mössbauer spectra of $Co_xFe_{3-x}O_4$ (x = 0.0, 0.5, 1, 1.5, 2, 2.5) samples at 4.3 K (a) without and (b) with an external magnetic field of 5 T along γ-ray propagation direction, consisting of experimental data (black dots), overall theoretical fit (red), Fe^{3+} octahedral B-site (blue) and Fe^{3+} tetrahedral A-site subspectra (green).

Mössbauer spectra of spinels described by $Co_xFe_{3-x}O_4$ were recorded at 4.3 K with and without a magnetic field applied parallel to the γ-ray incidence direction. The spectra can be described with two sextet subspectra corresponding to Fe^{3+} on tetrahedrally (A-site) and octahedrally coordinated (B-site) lattice positions. Subspectra were reproduced via narrow hyperfine field distributions. Especially for intermediate Co fractions $x \approx 1$, the individual contributions are evident even without applying a magnetic field (fig. S7 a) to yield better subspectral resolution, as they result in pronounced fine structure of the spectral lines, due to their different average hyperfine magnetic field and isomer shift. For $x < 2$ enhanced spectral resolution could be obtained in the in-field measurements (fig S7 b) due to the antiparallel alignment of the A- and B-site sublattice. For higher values of x towards antiferromagnetic Co_3O_4, the lack in magnetic orientation does not allow improved resolution as compared to the zero-field spectra, wherefore experiments at 5 T were limited to the aforementioned Co-fractions. The resulting increase in spin frustration upon rising x is evident by the rising relative intensity of lines 2 and 5 in the in-field spectra. In this context, a relative intensity ratio $A_{23} \approx 0$ corresponds to perfect in-field alignment, while $A_{23} \approx 2$ translates to randomly oriented magnetic moments even when exposed to the magnetic field [1], usually indicative of an antiferromagnetic state.

For a quantitative analysis of ion site occupation, we study the ratio of A- to B-site subspectral area, which represents the number of Fe ions on the respective lattice position, as the fraction of recoil-free processes for Fe on tetrahedral and octahedral sites at low temperatures can be considered to be very

similar. [43,44] Due to the high octahedral site preference energy of Co^{3+} as compared to Co^{2+} and Fe^{3+}, Co^{3+} is often assumed to be located on the octahedral sites only.[2,3] Based on this consideration, inversion parameters as discussed in the main text can be estimated using the following equations:

For lower Co contents ($1 \leq x \leq 2$, $\alpha \leq 1$) the equation according to Murray *et al.* [4] applies:

$$Fe^{3+}_{1-\alpha}Co^{2+}_{\alpha}\,[Fe^{3+}_{2-x+\alpha}Co^{2+}_{1-\alpha}Co^{3+}_{x-1}]O^{2-}_{4}$$

For high Co contents ($2 \leq x \leq 3$, $\omega \leq x-3$) the equation according to Le Trong *et al.* [2] applies:

$$Fe^{3+}_{3-x-\omega}Co^{2+}_{x-2+\omega}[Fe^{3+}_{\omega}\,Co^{2+}_{3-x-\omega}Co^{3+}_{x-1}]O^{2-}_{4}$$

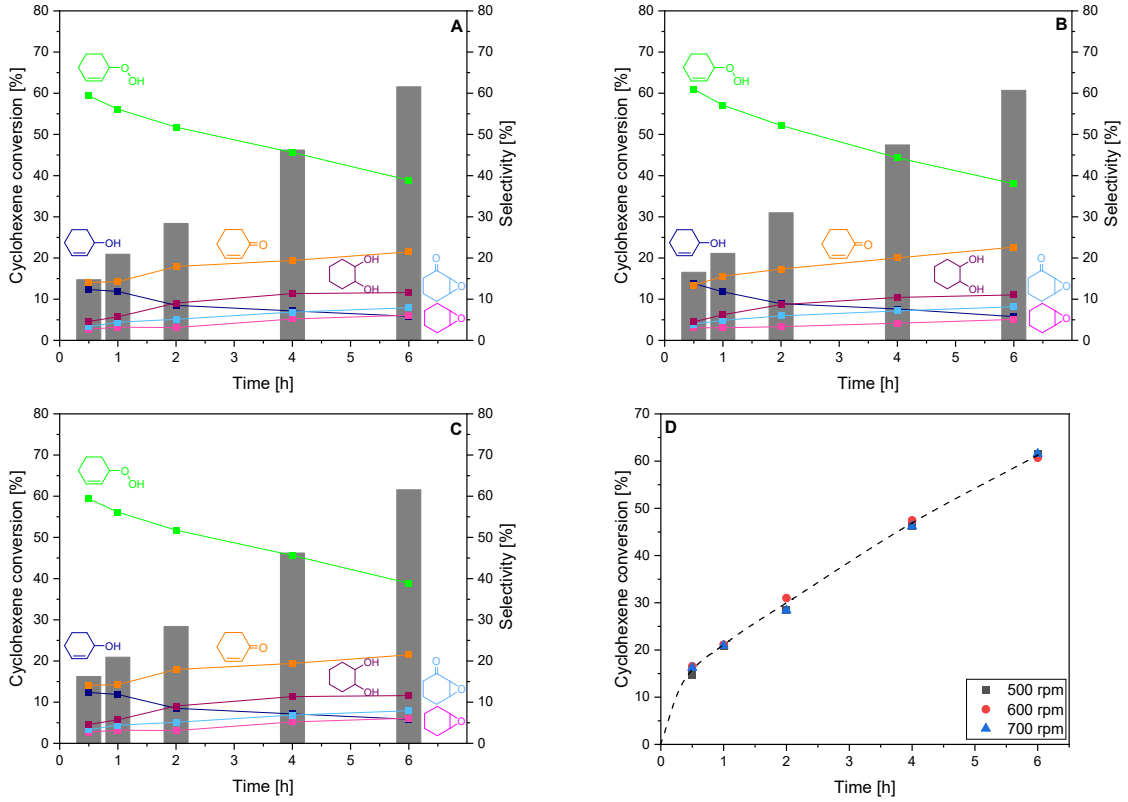

Figure S8. The effect of stirring speed on cyclohexene oxidation over $Co_{2.5}Fe_{0.5}O_4$ stirring with (A) 500, (B) 600 and (C) 700 rpm and (D) the comparison of cyclohexene conversion over time at different stirring speeds. Reaction conditions: 20 mmol cyclohexene, 30 mL acetonitrile, 50 mg $Co_{2.5}Fe_{0.5}O_4$, 10 bar O_2, 80 °C, 6 h.

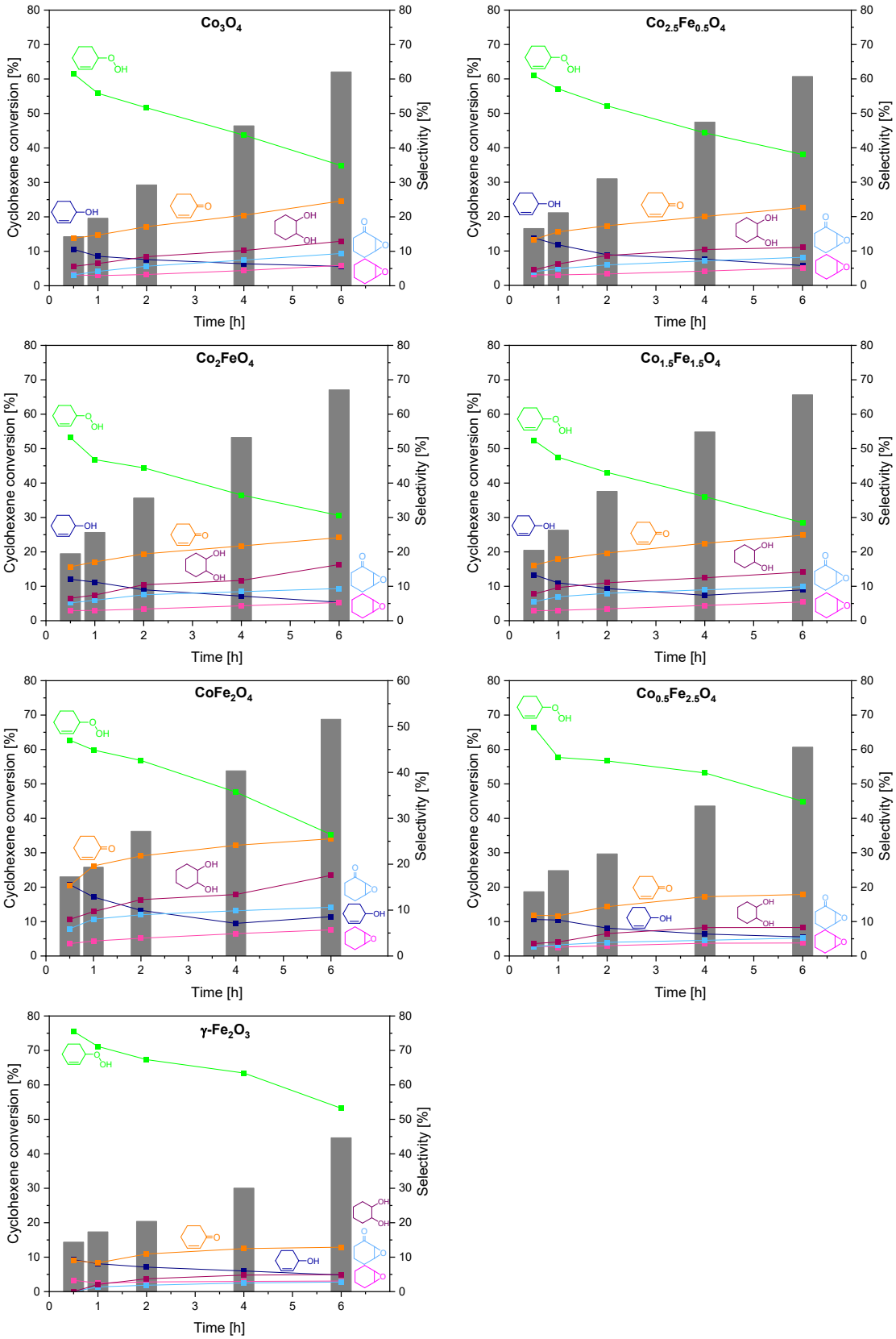

Figure S9. The influence of Fe doping on cyclohexene oxidation as a function of time over $Co_xFe_{3-x}O_4$ catalysts. Reaction conditions: 20 mmol cyclohexene, 30 mL acetonitrile, 50 mg catalyst, 80 °C, 10 bar O_2, 600 rpm, 6 h.

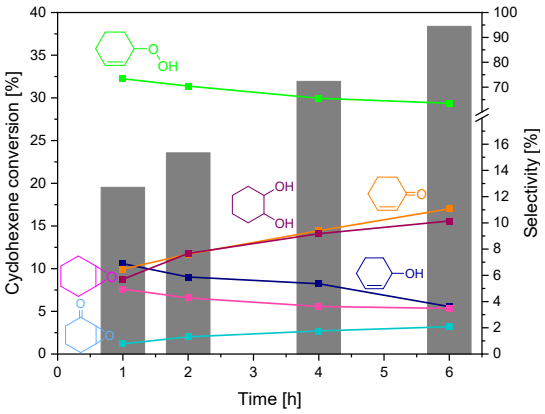

Figure S10. Cyclohexene conversion and product selectivity as a function of time in the absence of catalyst. Reaction conditions: 20 mmol cyclohexene, 30 mL acetonitrile, 80 °C, 10 bar O_2, 600 rpm, 6 h.

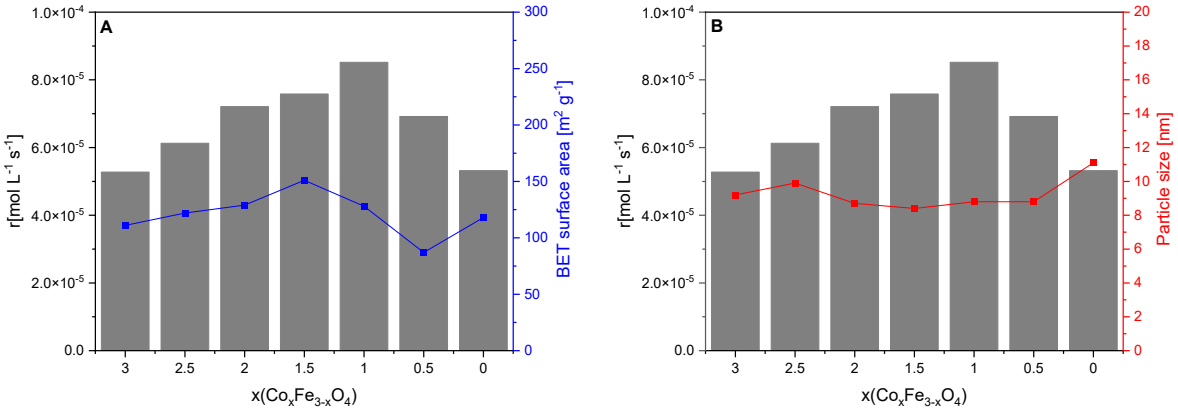

Figure S11. Effect of (A) specific surface area and (B) particle size on cyclohexene oxidation over $Co_xFe_{3-x}O_4$ catalysts. Reaction conditions: 20 mmol cyclohexene, 30 mL acetonitrile, 50 mg catalyst, 80 °C, 10 bar O_2, 600 rpm, 0.5 h.

Table S2. Comparison of the catalytic activity of Co-based catalysts in literature.

Reference	Catalyst	Reaction conditions	X [%]	S(Ketone) [%]
Present study	Spray-flame-synthesized $CoFe_2O_4$	0.67 mol L^{-1} 50 mg catalyst 80 °C 10 bar O_2 6 h	69	26
Büker et al.[5]	Spray-flame-synthesized $LaCoO_3$	0.67 mol L^{-1} 60 mg catalyst 80 °C 10 bar O_2 6 h	69	47
Denekamp et al.[6]	Co/N:C	1.65 mol L^{-1} 10 mg catalyst 70 °C 10 bar O_2 16 h	80	38
Fu et al.[7]	Co-MOF	5 mL cyclohexene (solvent-free) 50 mg catalyst 80 °C Ambient pressure 10 h	8	4
Silva et al.[8]	Deposited CoO	1.33 mol L^{-1} 0.004 mmol Co 75 °C 3 bar O_2 6 h	17	94
Silva et al.[8]	Deposited SiO_2-Co_3O_4	1.33 mol L^{-1} 0.004 mmol Co 75 °C 3 bar O_2 6 h	15	66
Sun et al.[9]	Co/Ni-MOF	2 mL cyclohexene 20 mg catalyst 80 °C Ambient pressure 20 h	55	30
Zhang et al.[10]	Co-MOF	18 mmol cyclohexene 0.05 mmol Co in MOF 70 °C Ambient pressure 24 h	38	20
Li et al.[11]	Co^{2+} supported on etched halloysite nanotubes	0.8 mL cyclohexene 40 mg catalyst 75 °C Ambient pressure 18 h	10	46

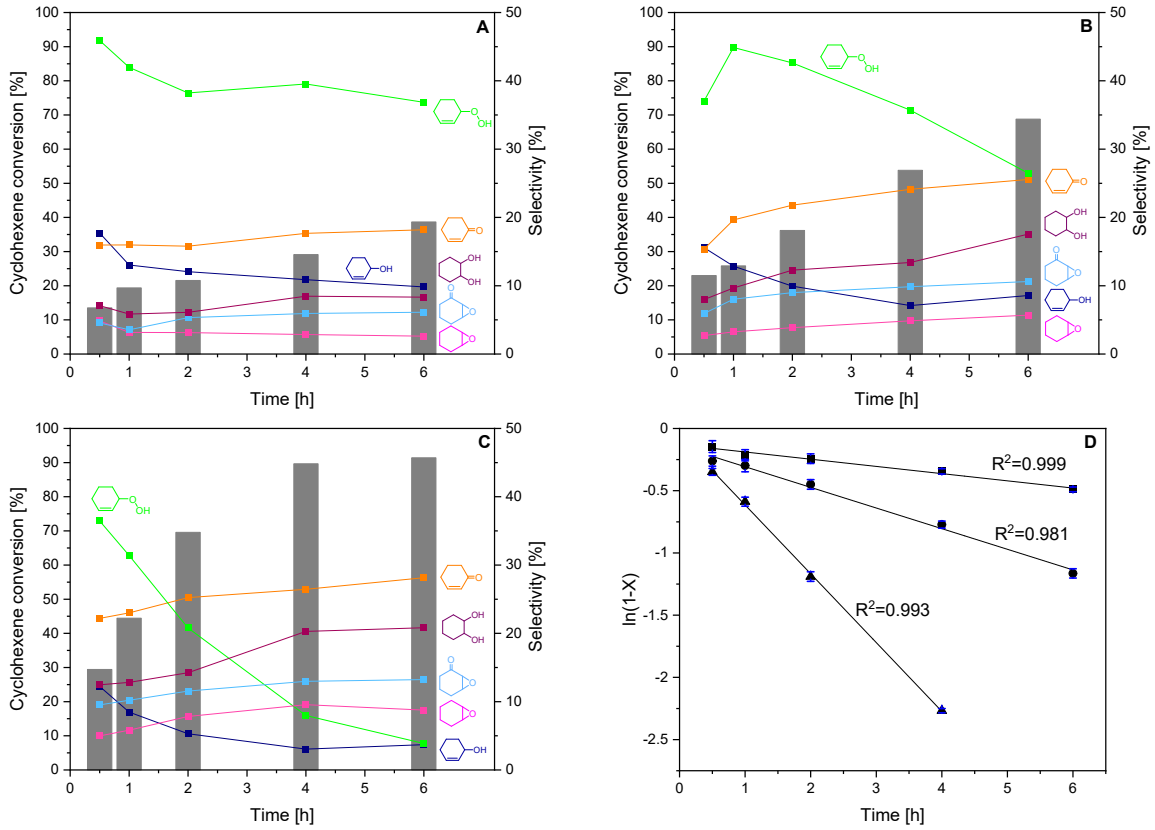

Figure S12. Cyclohexene oxidation over $CoFe_2O_4$ at (A) 60 °C, (B) 80 °C and (C) 100 °C and the linearized plot for Arrhenius analysis (D). Reaction conditions: 20 mmol cyclohexene, 30 mL acetonitrile, 50 mg catalyst, 10 bar O_2, 600 rpm, 6 h.

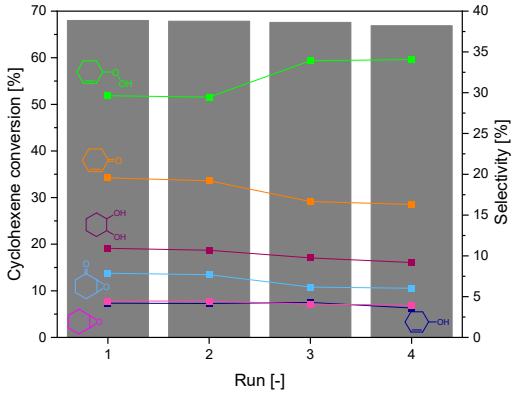

Figure S13. Reusability test of cyclohexene oxidation over $CoFe_2O_4$. Reaction conditions: 20 mmol cyclohexene, 30 mL acetonitrile, 50 mg catalyst, 80 °C, 10 bar O_2, 600 rpm, 6 h. After each run, the catalyst was separated by centrifugation and dried overnight at 60 °C.

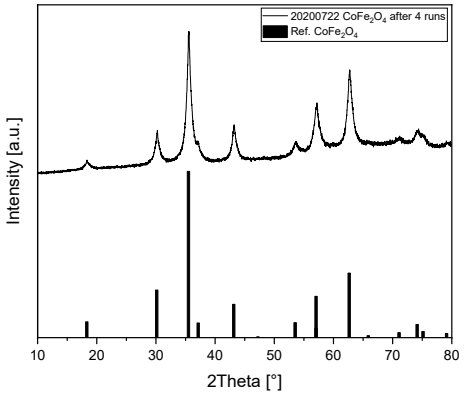

Figure S14. XRD pattern of $CoFe_2O_4$ after the reusability test with four consecutive reaction runs.

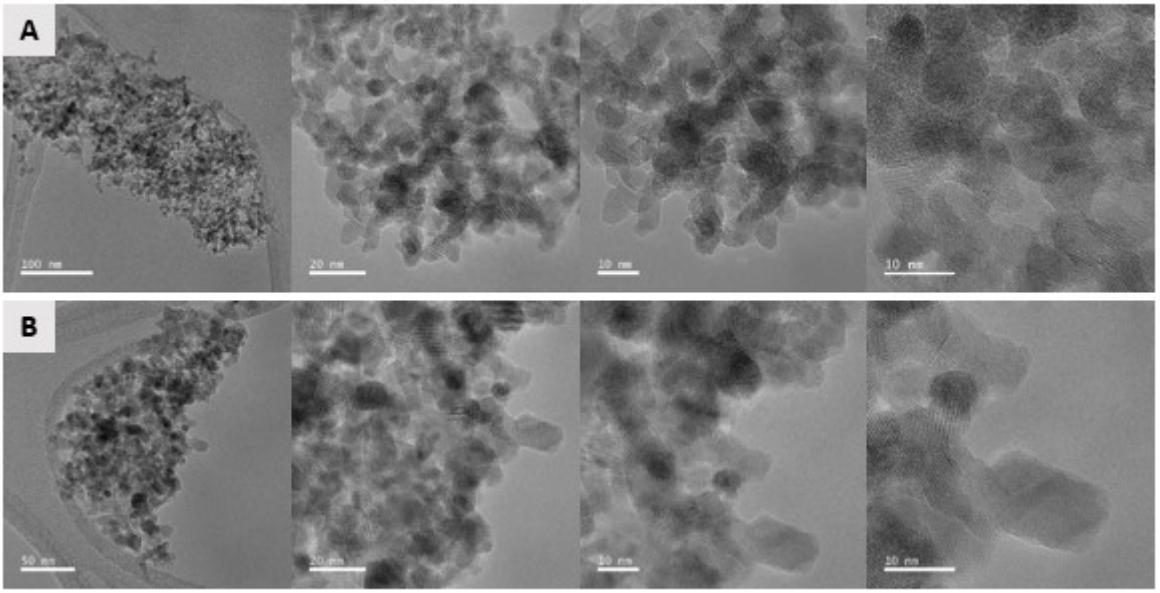

Figure S15. TEM images of $CoFe_2O_4$ before (A) and after (B) the reusability test with four consecutive reaction runs.

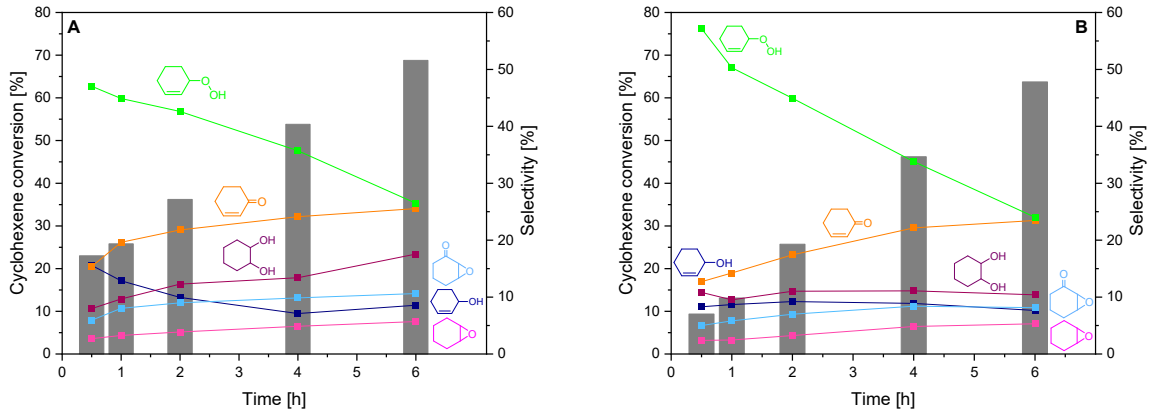

Figure S16. The influence of H_2O on cyclohexene oxidation; Cyclohexene conversion and product selectivity over $CoFe_2O_4$ in the absence (A) and in the presence (B) of H_2O. Reaction conditions: 20 mmol cyclohexene, 30 mL acetonitrile, 50 mg catalyst, 80 °C, 600 rpm, 6 h.

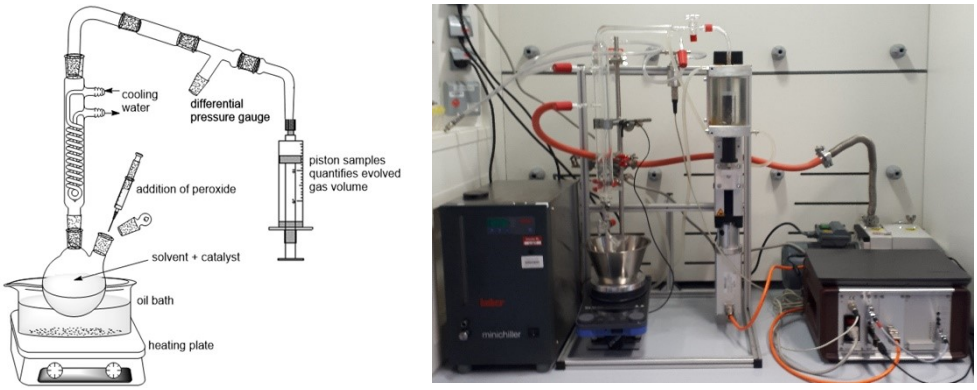

Figure S17. Scheme and picture of the peroxide decomposition set-up used for the simulation of hydroperoxide decomposition during cyclohexene oxidation using H_2O_2 and *tert*-butyl hydroperoxide.

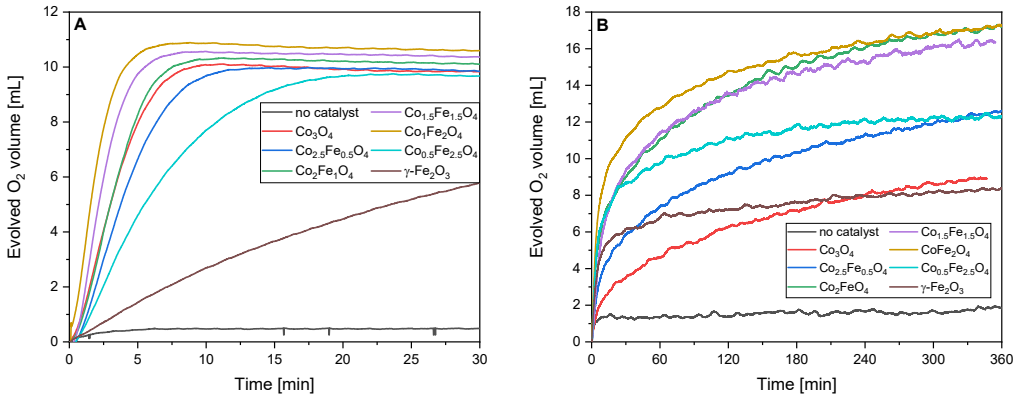

Figure S18. H_2O_2 (A) and TBHP (B) decomposition over $Co_xFe_{3-x}O_4$ catalysts. The reaction progress was monitored by recording the evolved O_2 volume over time.

Table S3. Reaction rate constants on H_2O_2 decomposition (0.04 M, 30 °C) over $Co_xFe_{3-x}O_4$ without normalization and normalized to the catalyst mass and specific surface area.

x	k [s^{-1}]	k_m [s^{-1} g^{-1}]	k_S [s^{-1} m^{-2}]
3	0.416	41.6	0.352
2.5	0.302	30.2	0.347
2	0.530	53.0	0.414
1.5	0.666	66.5	0.441
1	0.679	67.9	0.527
0.5	0.144	14.4	0.118
0	0.029	2.9	0.026
blank	0.00118	-	-

Table S4. Reaction rate constants on H_2O_2 decomposition over $CoFe_2O_4$ from literature.

Reference	c(H_2O_2)	T [° C]	Solvent	k
Cota et al.[46]	0.09 M H_2O_2	22	6.9 M KOH	k_S = 0.071 s^{-1} m^{-2}
Goldstein et al.[47]	1 M H_2O_2	25	5 M KOH	k_S = 0.120 s^{-1} m^{-2}
Mimani et al.[49]	0.1 M H_2O_2	30	H_2O	k_S = 0.232 s^{-1} m^{-2}
Onuchukwu et al.[48]	0.5 M H_2O_2	27	5 M KOH	k_m = 14 s^{-1} g^{-1}
Preeti et al. [50]	0.8 M H_2O_2	30	H_2O	k_m = 0.037 s^{-1} g^{-1}
Tatarchuk et al. [51]	0.02 M H_2O_2	25	H_2O	k_S = 0.04 s^{-1} m^2

Table S5. Theoretical spinel type and cationic distribution of the $Co_xFe_{3-x}O_4$ spinel series.[48],[49],[52]-[54]

x	Theoretical spinel type	Theoretical cation valency distribution*
3 (Co_3O_4)	Normal	(Co^{2+}) $[Co^{3+}{}_2]$
2.5		(Co^{2+}) $[Co^{3+}{}_{1.5}Fe^{3+}{}_{0.5}]$
2		(Co^{2+}) $[Co^{3+}Fe^{3+}]$
1.5	Inverse	$(Co^{2+}{}_{0.5}\ Fe^{2+}{}_{0.5})$ $[Co^{2+}{}_{0.5}\ Co^{3+}{}_{0.5}Fe^{3+}{}_{0.5}]$
1 ($CoFe_2O_4$)		(Fe^{3+}) $[Co^{2+}Fe^{3+}]$
0.5		(Fe^{3+}) $[Co^{2+}{}_{0.5}Fe^{2+}{}_{0.5}\ Fe^{3+}]$
0 (Fe_3O_4)		(Fe^{3+}) $[Fe^{2+}Fe^{3+}]$

*( ) and [ ] denote tetrahedral and octahedral coordinations sites, respectively

Scheme S1. Haber-Weiss reaction mechanism for H_2O_2 decomposition over Fe^{2+}.[55],[56]

$$Fe^{2+} + H_2O_2 \rightarrow Fe^{3+} + OH^- + HO^\bullet \quad (1)$$

$$H_2O_2 + HO^\bullet \rightarrow H_2O + HO_2^\bullet \quad (2)$$

$$Fe^{3+} + HO_2^\bullet \rightarrow Fe^{2+} + O_2 + H^+ \quad (3)$$

$$Fe^{2+} + HO_2^\bullet \leftrightarrow Fe^{3+} + HO_2^- \quad (4)$$

$$Fe^{2+} + HO^\bullet \leftrightarrow Fe^{3+} + OH^- \quad (5)$$

References

[1] J. Landers, S. Salamon, S. Webers, H. Wende, Microscopic understanding of particle-matrix interaction in magnetic hybrid materials by element-specific spectroscopy, *Phys. Sci. Rev.* 2021, https://doi.org/10.1515/psr-2019-0116

[2] H. Le Trong, L. Presmanes, E. de Grave, A. Barnabé, C. Bonningue, P. Tailhades, Mössbauer characterisations and magnetic properties of iron cobaltites CoxFe3− xO4 (1≤ x≤ 2.46) before and after spinodal decomposition, *J. Magn. Magn. Mater.* 2013, **334**, 66–73.

[3] D.S. McClure, The distribution of transition metal cations in spinels, *J. Phys. Chem. Solids* 1957, **3** ,311–317.

[4] P.J. Murray, J.W. Linnett, Mössbauer studies in the spinel system CoxFe3− xO4, *J. Phys. Chem. Solids* 1976, **37**, 619–624.

[5] J. Büker, B. Alkan, Q. Fu, W. Xia, J. Schulwitz, D. Waffel, T. Falk, C. Schulz, H. Wiggers and M. Muhler, Selective Cyclohexene Oxidation with O2, H2O2 and Tert-Butyl Hydroperoxide over Spray-Flame Synthesized LaCo1−xFexO3 Nanoparticles, *Catal. Sci. Technol.*, 2020, **10**, 5196–5206.

[6] I. M. Denekamp, M. Antens, T. K. Slot, G. Rothenberg, Selective Catalytic Oxidation of Cyclohexene with Molecular Oxygen: Radical Versus Nonradical Pathways, *ChemCatChem* 2018, **10**, 1035-1041.

[7] Y. Fu, D. Sun, M. Qin, R. Huang, Z. Li, Cu(II)-and Co(II)-containing metal–organic frameworks (MOFs) as catalysts for cyclohexene oxidation with oxygen under solvent-free conditions, *RSC Adv.*, 2012, **2**, 3309-3314.

[8] F. P. Silva, M. J. Jacinto, R. Landers, L. M. Rossi, Selective Allylic oxidation of Cyclohexene by a Magnetically Recoverable Cobalt Oxide Catalyst, *Catal Lett* 2011, **141**, 432-437.

[9] D. Sun, F. Sun, X. Deng, Z. Li, Mixed-Metal Strategy on Metal–Organic Frameworks (MOFs) for Functionalities Expansion: Co Substitution Induces Aerobic Oxidation of Cyclohexene over Inactive Ni-MOF-74, *Inorg. Chem.* 2015, **54**, 8639−8643.

[10] T. Zhang, Y.-Q. Hu, T. Han, Y.Q. Zhai, Y.-Z. Zheng, Redox-Active Cobalt(II/III) Metal–Organic Framework for Selective Oxidation of Cyclohexene, *ACS Appl. Mater. Interfaces* 2018, **10**, 18, 15786-15792.

[11] C. Li, Y. Zhao, T. Zhu, Y. Li, J. Ruan, G. Li, Effective solvent-free oxidation of cyclohexene to allylic products with oxygen by mesoporous etched halloysite nanotube supported Co^{2+}, *RSC Adv*. 2018, **8**, 14870.